

Seasonal and inter-annual variability of chlorophyll-*a* concentration in the Mauritanian upwelling: Observation of an anomalous event during 1998–1999

Yaswant Pradhan^{a,c,*}, Samantha J. Lavender^{a,c},
Nick J. Hardman-Mountford^{b,c}, James Aiken^{b,c}

^aSEOES, University of Plymouth, Plymouth PL4 8AA, UK

^bPlymouth Marine Laboratory, Plymouth PL1 3DH, UK

^cCentre for observation of Air–Sea Interactions and fluxes (CASIX), UK

Received 2 August 2005; received in revised form 9 February 2006; accepted 12 May 2006

Available online 10 August 2006

Abstract

Monthly chlorophyll-*a* (Chl-*a*) concentrations derived from SeaWiFS data for 1997–2005 and chlorophyll measurements from the Atlantic Meridional Transect for 1995–2001 have been analysed to describe seasonal and inter-annual variability of surface Chl-*a* in the Mauritanian upwelling. There was a moderate to strong correspondence between the seasonal cycles of surface Chl-*a* and the seasonal cycles of ocean physical and meteorological fields (such as sea-surface temperature, sea-surface height, and prevailing wind), with a noticeable exception in 1998 that corresponded to a strong anomalous Chl-*a* event (~250% increase) in the Mauritanian upwelling. Alongshore wind-stress and wind-stress curl were found to be the most significant factors controlling the variability of Chl-*a* (jointly explaining more than 50% of total variance). The biological response to the alongshore wind-stress was immediate, but it lagged the wind-stress curl by 1–2 months (each explaining more than 40% of the total Chl-*a* variability). These observations also demonstrate a link, hitherto unreported, between the Pacific El-Niño Southern Oscillation (ENSO) and anomalous Chl-*a* field in the Mauritanian upwelling. The multivariate ENSO index was shown to account for a significant part of the variability of the autumn–winter Chl-*a* anomaly ($r = -0.52$, $p < 0.01$). A cold event, following an intense El Niño in the Pacific during summer, was found to mirror the intensity of wind forcing and phytoplankton concentration in the Mauritanian upwelling a few months later. Therefore, ENSO-related changes in the local atmospheric fields are considered as the preferred candidates for explaining the observed biological changes in the Mauritanian upwelling during 1998–1999.

© 2006 Elsevier Ltd. All rights reserved.

Keywords: Mauritanian upwelling; Chlorophyll-*a*; ENSO; Seasonal variations; Time-series; AMT

1. Introduction

Upwelling ecosystems associated with Eastern boundary currents (EBC) are characterised by high phytoplankton production (Carr, 2001) and high levels of spatial and temporal variability

*Corresponding author. SEOES, University of Plymouth, Plymouth PL4 8AA, UK. Tel.: +44 1752 232 435; fax: +44 1752 232 406.

E-mail address: yaswant.pradhan@plymouth.ac.uk (Y. Pradhan).

(Hill et al., 1998). Over seasonal and inter-annual time scales, this variability may have significant implications for carbon-cycling in the oceans and the sustainability of commercially important fish populations.

The Atlantic Meridional Transect (AMT) programme sampled the surface ocean between the UK and Falkland Islands twice yearly (Aiken and Bale, 2000). The Mauritanian upwelling (Fig. 1), 10–25°N and between 30°W to the northwest African coast, is traversed by these AMT tracks. Persistent north-easterly trade winds drive upwelling along the northwest African coast and, with the *Canary Current* (Zhou et al., 2000) (Fig. 1), determine the phytoplankton distribution in the Mauritanian upwelling system. The *Canary Current* is characterised by strong seasonal variability and a sharp contrast in the biology (phytoplankton blooms) between northern and southern waters (Sætersdal et al., 1999). The study area also covers the Guinea Dome (centred near 22°W and 12°N) in the south (Fig. 1) that results from the interaction of the eastward-flowing *North Equatorial Counter Current*

and the westward-flowing *North Equatorial Current* (Yamagata and Iizuka, 1995).

The surface chlorophyll seasonal variability in the four major EBC systems was described by Thomas et al. (2001b; 2004), using Coastal Zone Colour Scanner (CZCS) and Sea viewing Wide Field-of-view Sensor (SeaWiFS) data. They reported that the peak high and low concentrations in the *Canary Current* were located at 10–20°N and ~35°N, respectively. Signorini et al. (1999) described the spatio-temporal variability of surface chlorophyll (observed by SeaWiFS) in the tropical Atlantic during the 1997–1998 El Niño–La Niña transition. They observed anomalous changes in physical and biological properties throughout the eastern tropical Atlantic, but inter-annual anomalies in the Mauritanian upwelling were not discussed.

The inter-relationships between Pacific El-Niño Southern Oscillation (ENSO) and local anomalies of hydro-meteorological fields in different parts of the globe have been studied extensively in recent years. In a recent study, Larkin and Harrison (2005) showed the influence of ENSO on global seasonal temperature and precipitation. ENSO-related hydrographic and phytoplankton anomalies have been reported extensively for Pacific EBCs (Chavez et al., 1999; Thomas et al., 2001a; Thomas et al., 2004). The relationship between boreal winter El-Niño sea-surface temperature (SST) anomaly and boreal spring tropical SST gradient was investigated by Huang et al. (2005). An ENSO-related coastal SST anomaly in the eastern Atlantic was also linked to the variability in annual catches of sardine (Roy and Reason, 2001). Most of these reports relate ENSO to SST or precipitation anomalies. However, a comprehensive study of the seasonal and inter-annual variability of coupled bio-physical processes in the Mauritanian upwelling (including the anomalies during the ENSO period) has not been published to date.

In this paper, the seasonal and inter-annual variability of surface chlorophyll-*a* (Chl-*a*) in the Mauritanian upwelling was investigated using more than 8 years of Earth observation (EO) data combined with in situ observations from the AMT cruises. The major goals of this paper are (i) to quantify relationships between observed Chl-*a* and local wind forcing (alongshore wind-stress (τ_y) and wind-stress curl ($\nabla \times \tau$)) and (ii) to investigate links between the 1997–1998 ENSO and the anomalies observed in the Mauritanian upwelling.

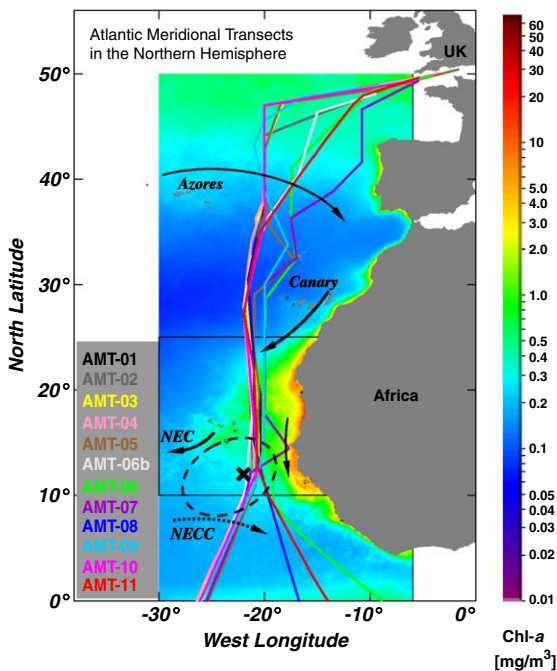


Fig. 1. AMT (1995–2001) in the northern hemisphere (shown as coloured lines) overlaid on the 8-year (1997–2005) mean SeaWiFS Chl-*a* map. The arrows represent major current systems (see text). The Mauritanian upwelling zone (10–25°N, 30°W to coast) is defined by the box and the Guinea Dome (12°N, 22°W) is shown by the dashed oval.

2. Data and methods

2.1. Earth observation data

SeaWiFS Chl-a: Level-3 mapped monthly mean SeaWiFS global 9-km Chl-*a* data (reprocessing version 5.1) were downloaded from National Aeronautics and Space Administration (NASA) Ocean-color website (<ftp://oceans.gsfc.nasa.gov/SeaWiFS/L3SMI/>). The Chl-*a* maps were generated using the fourth generation Maximum Band Ratio algorithm, OC4v4, that yields a reasonably good correlation ($r^2 = 0.892$) and small error (RMS = 0.222) on a global scale that includes samples from all water types (O'Reilly et al., 2000). Generally, the satellite-derived Chl-*a* measurement represents the mean value for the surface layer derived from the upwelling radiance from the surface to first attenuation depth, heavily weighted towards the surface.

ERS-2 and QuikSCAT vector wind: Weekly gridded European Remote-Sensing Satellite-2 (ERS2) and NASA-QuikSCAT (QS) mean wind fields (MWF) at 0.5° resolution were obtained through an anonymous FTP (<ftp://ftp.ifremer.fr/ifremer/cersat/products/gridded/>). A comparison between ERS2 and QS wind speeds showed good agreement, but a systematic bias was found over the Mauritanian upwelling showing an under-estimation of ERS2 wind speed compared to QS wind speed. Based on the concurrent (August 1999–December 2000) datasets from both sensors, the difference was adjusted to best fit the QS wind; it was assumed that QS performed better than ERS2 since the mean estimation error (provided with the MWF product) for QS wind (0.25 ms^{-1}) is significantly smaller than for ERS2 wind (0.55 ms^{-1}). A detailed discussion is beyond the scope of this paper, but the correction involved the application of a linear scaling to the zonal and meridional components of ERS2 wind speed as

$$\begin{aligned} u &= 1.107u_{E2} + 0.4395 \quad \text{and} \\ v &= 1.065v_{E2} - 0.6332, \end{aligned} \quad (1)$$

where u and v are the corrected across-shore (zonal) and alongshore (meridional) wind speed components, and u_{E2} and v_{E2} are the respective ERS2 wind speed components. The wind-stress (τ) was calculated using variable drag coefficients (C_D) (Yelland and Taylor, 1996)

$$\tau = \rho_a C_D |W|W, \quad (2)$$

where $\rho_a \approx 1.3 \text{ kg m}^{-3}$ (average air density) and W is the wind speed.

$$C_D = \left(0.29 + \frac{3.1}{W} + \frac{7.7}{W^2} \right) 10^{-3} \quad \text{for} \\ (3 \leq W \leq 6 \text{ ms}^{-1})$$

$$C_D = (0.6 + 0.07W) 10^{-3} \quad \text{for} \\ (6 \leq W \leq 26 \text{ ms}^{-1}) \quad \text{or} \quad C_D = 10^{-4}, \quad \text{otherwise.}$$

The 9-year (1997–2005) monthly wind parameter (wind speed, wind-stress and wind-stress curl) time-series was constructed using both ERS2 and QS after applying this correction (Eq. (1)) to the ERS-2 data.

Additional EO and climatological data: The Reynolds Optimally Interpolated SST dataset (Reynolds and Smith, 1994) is based upon a combination of advanced very high-resolution radiometer satellite and in situ data¹, available from the NASA Physical Oceanography Distributed Active Archive Center (PO.DAAC Product #119). The $1/3^\circ$ merged (TOPEX/Poseidon, Jason and ERS1/2) altimeter sea-level anomaly (SLA) data were produced and provided by the enhanced ocean data assimilation and climate prediction project (EVK2-CT2001-00117), and are available via an anonymous FTP (<ftp://ftp.cls.fr/pub/oceano/enact/msla/merged/>).

Bimonthly multivariate ENSO index (MEI) data for the 1997–2005 period, available from the NOAA Climate Diagnostics Centre (www.cdc.noaa.gov/people/klaus.wolter/MEI/), were used to verify the large-scale atmospheric modulation on the phytoplankton variability in the study area. All MEI values are normalised for each bimonthly period so that the 44 values (from 1950 to 1993) have zero mean and unit variance (Wolter, 2006). The MEI was used since it integrates more information than the Southern Oscillation Index or various SST indices; it reflects the nature of the coupled ocean–atmosphere system better than either component and it is less vulnerable to occasional data glitches in the monthly update cycles (Wolter, 2006).

2.2. In situ data

To obtain the vertical distribution of Chl-*a*, data from fluorometers attached to the AMT conductivity–temperature–depth (CTD) frame were used.

¹ftp://podaac.jpl.nasa.gov/pub/sea_surface_temperature/reynolds/oisst/doc/oisst.html#17 and the references therein

The fluorometer data were calibrated at the British Oceanographic Data Centre (BODC) using the fluorometric Chl-*a* measurements made on CTD bottle samples. CTD bottle samples were also analysed to estimate the total Chl-*a* (Tchl-*a*) concentration using the high-performance liquid chromatography (HPLC) technique (Aiken et al., 1998); Tchl-*a* is the sum of chlorophyllide-*a*, Chl-*a* epimer, Chl-*a* allomer, monovinyl Chl-*a* and divinyl Chl-*a* (Mueller et al., 2003). Tchl-*a* values were then averaged over the top 15 m in the Mauritanian upwelling region.

All the HPLC data collected during AMT cruises were obtained from the SeaWiFS Bio-optical Archive and Storage System (SeaBASS) public access database (http://seabass.gsfc.nasa.gov/cgi-bin/pigment_search.cgi). Available nutrient data ($\text{NO}_3 + \text{NO}_2$ concentration by colorimetric auto-analysis method), particulate organic nitrogen (PON) and CTD profile data were collected on AMT cruises and provided by BODC.

2.3. EO data analysis

For all latitude–time cross-sections described in this paper, the monthly (and reconstructed monthly) EO data were pre-interpolated to a $1^\circ \times 1^\circ$ grid space using a kriging method (Stein, 1999). Monthly anomalies were then computed as departures from 8-year (1998–2005) mean monthly values. Before constructing the spatially averaged time-series, each anomaly data cube (longitude, latitude and time) was standardised over time so that the data in each grid point, in the entire monthly time-series (1997–2005), have an average of ‘0’ and a standard deviation of ‘1’. The strength and direction of the relationship between surface Chl-*a* (prediction) variability and the forcing fields (explanatory) were evaluated using Spearman’s rank correlation coefficient as it provides a credible result when the sample size is relatively small (Altman, 1991). The combined effect of all independent variables (only strength) also was determined through multiple correlation analysis (Huberty, 2003).

3. Results

The meridional cross-section (zonally averaged) of SeaWiFS estimated Chl-*a* concentration in the Mauritanian upwelling, between 10 and 20°N, showed a strong seasonal cycle dominated by a

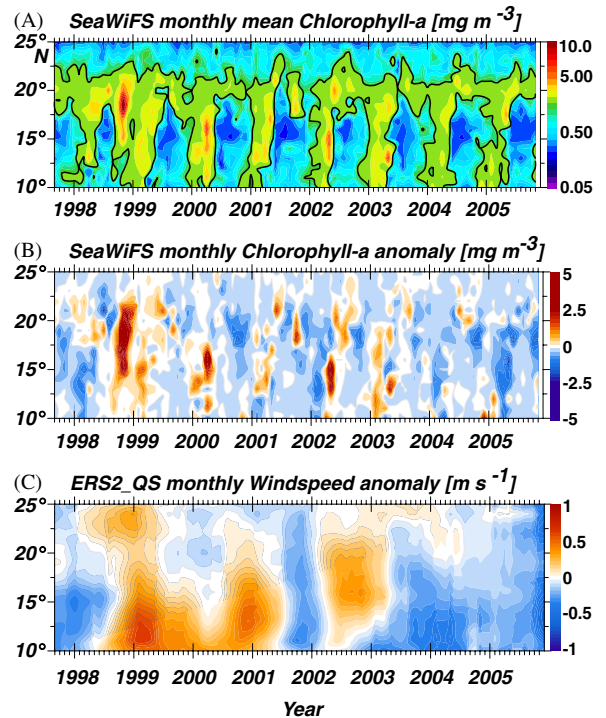


Fig. 2. Zonally averaged (30°W–NW African coast) time–latitude plots of (A) monthly mean SeaWiFS Chl-*a* (values $> 1.0 \text{ mg m}^{-3}$ are shown as bold contour), (B) SeaWiFS monthly Chl-*a* anomalies from mean monthly Chl-*a* values for the 8-year period (1998–2005) and (C) same as B, but for the reconstructed ERS2_QS wind speed anomaly (see methods).

spring peak (Fig. 2A). Elevated concentrations ($> 1.0 \text{ mg m}^{-3}$) were present from January–May and typically peaked (up to $\sim 8.0 \text{ mg m}^{-3}$) in February–March in the south and April–May further north. Around 20°N, elevated Chl-*a* concentrations persisted throughout the year; it is around this latitude that the main branch of the *Canary Current* leaves the African coast. This seasonal cycle of Chl-*a* was consistent throughout the time series, with the exception of 1998 when an anomalous second peak of greater magnitude was observed from September to December. A time–latitude plot of Chl-*a* anomalies (Fig. 2B) showed the magnitude of this anomalous event ($> 2.5 \text{ mg m}^{-3}$).

To validate the observed Chl-*a* anomaly, latitude–depth sections from AMT cruises were examined (Fig. 3). These revealed a 2–3 times enhancement of Chl-*a* concentration between 10 and 22°N, during spring and autumn 1998 as compared with other years. In contrast, the surface signature as estimated by satellite showed only autumn 1998 values to be

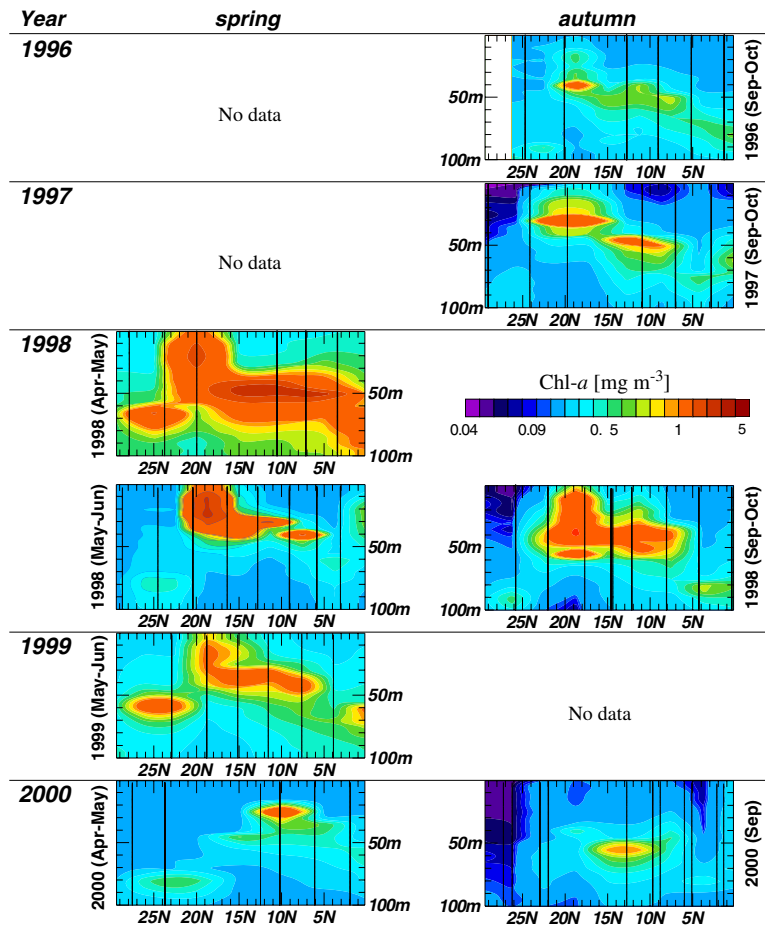


Fig. 3. Vertical structure (latitude–depth) of seasonal (spring and autumn) Chl-*a* (CTD fluorometer profiler) concentration observed during AMT campaigns (1996–2000). A nearest neighbourhood interpolation method was implemented to fill the data gaps between sampling stations (shown as vertical lines) in the latitudinal direction.

anomalously high (Fig. 2B). Even though the space–time sampling differences between the two methods are obvious, both showed major anomalies in 1998. The surface (0–15 m) in situ samples showed that, during 1998, elevated Tchl-*a* (from HPLC) coincided with 2–3 times rise in nutrient ($\text{NO}_3 + \text{NO}_2$) and PON levels (Fig. 4). The inter-annual variability of Chl-*a*, nutrients and PON were very similar ($r_{\text{Chl-}a, \text{nutrient}} = 0.7$, $p < 0.1$; $r_{\text{Chl-}a, \text{PON}} = 0.6$, $p = 0.1$). Particulate organic matter such as carbon (POC) and nitrogen (PON) comprise mostly faecal pellets and other detrital material (arising mainly from zooplankton grazing of phytoplankton), higher values occurring with higher phytoplankton biomass.

To investigate the relationship between the seasonal cycle of surface Chl-*a* and putative physical drivers (SST, wind-stress, alongshore wind-stress,

wind-stress curl and SLA), a cross-correlation analysis was performed on the mean fields for each variable. The strongest correlation was seen with meridional wind-stress (τ_y) without a time lag (Table 1). All the other physical variables showed modest correlations ($r > 0.6$) with Chl-*a* concentration (Table 1); the period of analysis was from 1999 to 2005 so that 1998 was not included. When 1998 was included, the seasonal correlations were substantially reduced ($r < 0.5$) for all variables.

To further investigate forcing of this anomalous event, time–latitude plots of anomalies in physical variables were examined. Wind speed anomalies (Fig. 2C) exceeding 0.5 m s^{-1} were observed throughout the whole region, from 10 to 25°N, during autumn–winter 1998. However, other anomalous wind events did not correspond to anomalous

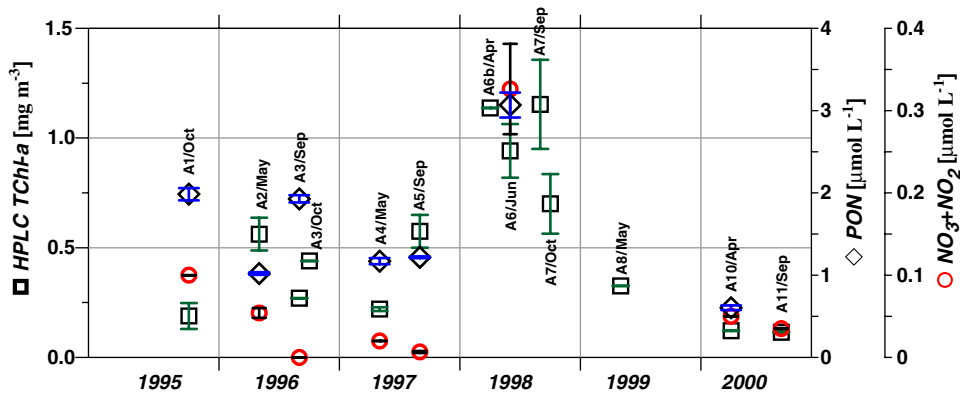


Fig. 4. Depth and time averaged (top 15 m, by cruise, by month) AMT 1995–2000 in situ measurements of HPLC Tchl-*a* (squares), nutrients ($\text{NO}_3 + \text{NO}_2$; circles) and PON (diamonds) in the Mauritanian upwelling (10–25°N, 30–10°W). The vertical bars indicate $\pm 1\sigma$. All sampling stations pass through nearly the same transect close to 20°W (Fig. 1). Data from the inshore stations during AMT-07 were excluded from this analysis.

Table 1

Cross-correlation ($r_{[\text{lag}]}$) between monthly mean Chl-*a* concentration and the monthly means of physical variables (meridional wind-stress (τ_y), wind-stress (τ) and wind-stress curl ($\nabla \times \tau$) in the Mauritanian upwelling)

Period		τ_y	SST	τ	SLA	$\nabla \times \tau$
September 1997–November 2005	Chl- <i>a</i>	$r_{[0]} = 0.48$	$r_{[0]} = -0.19$	$r_{[0]} = 0.29$	$r_{[0]} = -0.31$	$r_{[0]} = 0.41$
		$r_{[1]} = 0.44$		$r_{[1]} = 0.33$	$r_{[-2]} = -0.43$	$r_{[1]} = 0.46$
January 1999–November 2005	Chl- <i>a</i>	$r_{[0]} = 0.79^*$	$r_{[0]} = -0.67^*$	$r_{[0]} = 0.64^*$	$r_{[0]} = -0.63^*$	$r_{[0]} = 0.64^*$
		$r_{[1]} = 0.72^*$		$r_{[1]} = 0.69^*$	$r_{[-2]} = -0.49$	$r_{[1]} = 0.72^*$

[$N = 12$; $df = N - (|\text{lag}| + 1)$. Correlations significant at 95% confidence limit are assigned with *].

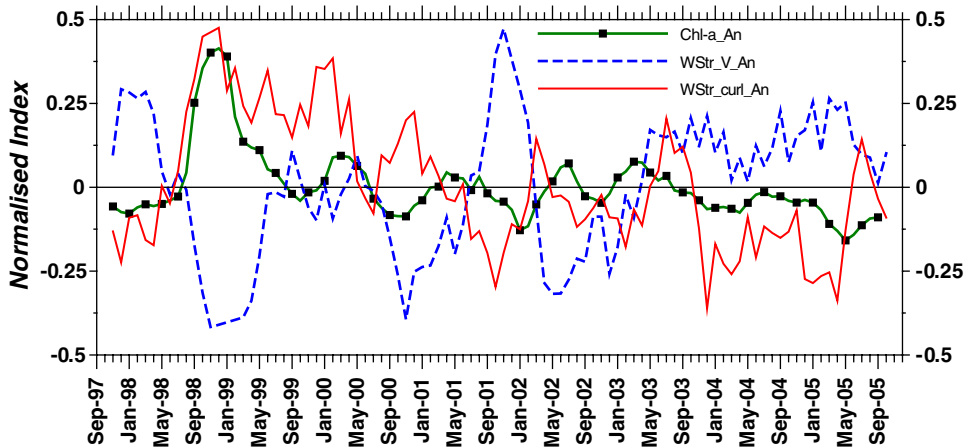


Fig. 5. Time evolution of SeaWiFS Chl-*a* anomaly (green line with filled squares), alongshore wind-stress anomaly (dashed blue line) and wind-stress curl anomaly (thin red line) in the Mauritanian upwelling. Each time-series was normalised by the maximum value of that series (for better scaling) and smoothed using a 3-month running average scheme.

chlorophyll events. No equivalent signal was observed in the SST anomaly and SLA plots (not shown).

To understand this relationship with wind forcing better, the standardised and spatially averaged time-series of Chl-*a* (dependent variable) was plotted

against alongshore wind-stress, τ_y , and wind-stress curl, $\nabla \times \tau$ (independent variables; Fig. 5). Together, τ_y and $\nabla \times \tau$ anomalies explained more than 50% of the Tch1-a anomaly's variability ($R = 0.71$;

Table 2
Correlation between $(\text{Chl-}a)_{\text{anomaly}}$ and alongshore wind-stress and wind-stress curl anomalies

Lag in months	r [τ_y vs. $\text{Chl-}a_{\text{anomaly}}$]	r [$\nabla \times \tau$ vs. $\text{Chl-}a_{\text{anomaly}}$]	R [(τ_y and $\nabla \times \tau$) vs. $\text{Chl-}a_{\text{anomaly}}$]
-3	-0.36	0.32	
-2	-0.48	0.39	
-1	-0.58	0.50	
0	-0.65	0.60	0.71
+1	-0.64	0.66	
+2	-0.57	0.66	
+3	-0.48	0.59	

R and r represent multiple- and cross-correlation coefficients, respectively. The degrees of freedom vary with lags in months as $N = 99 - (|\text{lag}| + 1)$. All correlations are significant at 99% confidence limit.

Table 3
Seasonal correlation between surface $(\text{Chl-}a)_{\text{anomaly}}$ and alongshore wind-stress and wind-stress curl anomalies

Season (boreal)	N	r (τ_y vs. $\text{Chl-}a_{\text{anomaly}}$)	r ($\nabla \times \tau$ vs. $\text{Chl-}a_{\text{anomaly}}$)
Autumn–winter (ONDJ)	32	-0.39	0.46*
Spring–summer (AMJJ)	30	-0.58*	0.51*

Correlation coefficients with $p < 0.01$ are shown with *.

Table 2). The maximum correlation between τ_y and $\text{Chl-}a$ anomaly occurred without a time lag ($r = -0.65$; $p < 0.001$), whereas $\text{Chl-}a$ anomaly was best correlated with $\nabla \times \tau$ anomaly at a 1–2 month lag ($r = 0.66$; $p < 0.001$). The seasonal decomposition, using the entire series, showed that τ_y could describe $\text{Chl-}a$ variability in spring–summer, whereas $\nabla \times \tau$ played a significant role in autumn–winter (Table 3).

Cross-correlation analysis showed that while the strength of the local wind-stress anomaly was in phase with the $\text{Chl-}a$ anomaly, the Pacific MEI was out-of-phase with the Mauritanian $\text{Chl-}a$ (and wind-stress) anomaly with a lag of about 2–3-months (not shown). The Mauritanian upwelling reached its southernmost extent in winter (Fig. 2) and the time-series of wintertime (November–December–January–February) $\text{Chl-}a$ anomaly and wind-stress anomaly were modestly correlated with a 3 month lag (corresponding to the 4-months September–December) with respect to the Pacific MEI. This was evident in the inter-annual time-series of mean wintertime (November–December–January–February) $\text{Chl-}a$, wind-stress anomalies and mean 4-monthly (September–October–November–December) MEI (Fig. 6). A correlation coefficient higher than -0.5 ($p < 0.01$) between the seasonal MEI and averaged $\text{Chl-}a$ anomaly indicated that the MEI was a statistically good predictor of the strength of Mauritanian upwelling phytoplankton variability, which is normally controlled by the prevailing wind field.

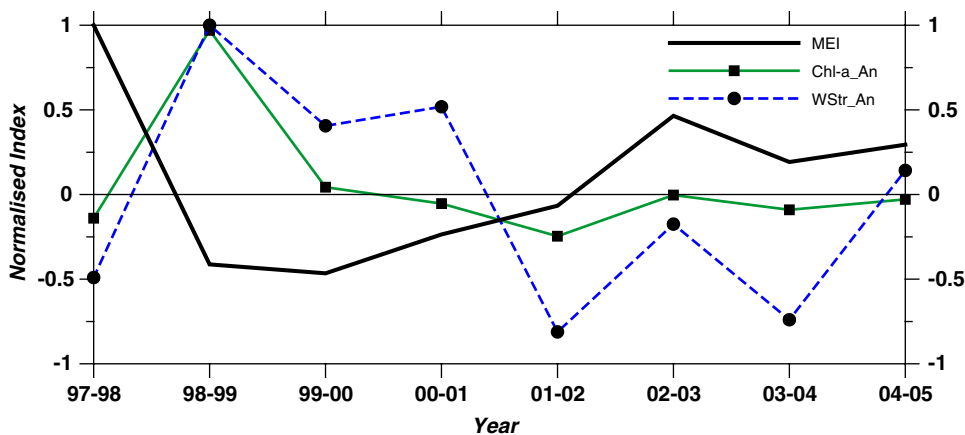


Fig. 6. Seasonally averaged (November–December–January–February) annual time-series of SeaWiFS $\text{Chl-}a$ anomaly (green line with filled squares) and wind-stress anomalies (dashed blue line with filled circles) in the Mauritanian upwelling and spring–autumn (September–October–November–December) multivariate ENSO index (thick black line). A 3-month lag is most significantly correlated with the out-of-phase pattern between the Pacific EMI and the Mauritanian $\text{Chl-}a$ anomaly ($r = -0.52$, $p < 0.01$)

4. Discussion

In this study, an almost 200-km stretch (10–20°N) of the North Atlantic Ocean along the northwest African coast was observed to have high Chl-*a* concentrations ($>1.0 \text{ mg m}^{-3}$) from January to May, typically peaking in April–May (Fig. 2A); this is different from the previously reported seasonal Chl-*a* maximum in May–June as observed from 1997–2000 monthly SeaWiFS data (Thomas et al., 2001b). An anomalously large Chl-*a* bloom was observed in 1998–1999 in both SeaWiFS (Fig. 2B) and in situ data (Figs. 3 and 4), which was not observed again in the full 1997–2005 SeaWiFS time-series (Fig. 5).

Phytoplankton blooms are modulated by variation of both nutrient and light availability apart from other factors (such as temperature, salinity, stratification and turbulence). The observed anticorrelation between SST and Chl-*a* concentration (Table 1) can be attributed to cold, upwelled, nutrient-rich water and the strong seasonal cycle that both SST and Chl-*a* follow. But the cold signature of the upwelled water may be confined to a local domain (inshore) and not clearly visible in SST data, particularly in a tropical region. On the other hand, Chl-*a* distribution can be very patchy, which may reflect the nature of the upwelling process. Thus, correlations with SST alone cannot be used effectively to predict the Chl-*a* field. Vertical fluxes of nutrient-rich water from below the nutricline to the ocean surface can be inferred from SLA field, because changes in the thermocline depth (often overlaps with the nutricline depth) are largely reflected in SLA. Satellite-derived surface Chl-*a* has been compared to SLA variability by many authors (Murtugudde et al., 1999; Cipollini et al., 2001; Siegel, 2001; Uz et al., 2001). But in a recent study, Wilson and Adamec (2002) showed that the correlation between Chl-*a* and SLA variability in the tropical Atlantic (including the Mauritanian upwelling) is non-significant. Thus, wind-induced upwelling supplies nutrients to enhance the Chl-*a* production. Strong southerly (negative) alongshore wind-stress would result in strong cross-shelf divergence along the eastern boundaries in the northern hemisphere and Ekman suction due to positive wind-stress curl is directly related to uplift of the pycnocline (Tomczak and Godfrey, 1994).

At low latitudes, seasonal blooms are triggered by an injection of nutrients from depth (less vertical stability) into the permanently warm mixed layer

(Dandonneau et al., 2004). The base of the mixed layer in the Mauritanian upwelling is quite shallow (about 15–25 m near 10–15°N) during summer (Monterey and Levitus, 1997), and the large-scale spatial wind structure in this region is also characterised by cyclonic wind-stress curl that contributes to an offshore extension of the coastal upwelling boundary (Bakun and Nelson, 1991). Consistent and prolonged alongshore wind-stress (τ_y) and wind-stress curl ($\nabla \times \tau$) could bring the deep pool of nutrients to the surface, enhancing the Chl-*a* concentration in the euphotic layer in this region. A primary source of the inter-annual variability of upwelling signal for the North Atlantic is the region of NW Africa in the vicinity of the Guinea dome (McClain and Firestone, 1993). Dynamic uplifting of the thermocline is a common feature in the Guinea Dome, which follows the quasi-geostrophic adjustment in response to the wind curl forcing (Signorini et al., 1999). The AMT transects cross near the Guinea dome at 12°N, which could have provided additional information on an anomalous elevation (doming) of the thermohaline structure that in turn could have caused the injection of nutrients from the nutricline. Although an ocean general circulation model showed a shallowing of the 20°C isotherm by 30–40 m from the middle of February until the beginning of September (in 1998) in the eastern tropical Atlantic (Signorini et al., 1999), the AMT in situ hydrographic (temperature and salinity) sections did not show any significant changes compared to other years (not shown). The in situ sampling station positions may be too widely spaced to resolve the thermohaline changes near the Guinea Dome.

An assumption that Chl-*a* concentration is directly proportional to the upwelling strength was justified as both τ_y and $\nabla \times \tau$ anomalies explained more than 50% of the Tchl-*a* anomaly's variability (Table 2). Though the prevailing alongshore wind field was generally favourable for coastal upwelling throughout the year, the seasonal decomposition showed that τ_y (potentially triggering the coastal upwelling) is a key forcing function to describe the Chl-*a* variability in spring–summer, whereas $\nabla \times \tau$ (potentially triggering the Ekman suction) plays a significant role in autumn–winter (Table 3). Following the large changes in 1998–1999, the Chl-*a* anomaly followed a near-regular annual oscillation until 2003 that was coherent with the wind fields (Fig. 5). In the subsequent years, Chl-*a* anomalies remained consistently below normal and in phase

with positive τ_y anomalies (i.e. weak southerly) and negative $\nabla \times \tau$ anomalies.

Although the wind-driven coastal upwelling of nutrient-rich subsurface water (on a regional scale) makes the EBC systems among the most biologically productive regions of the global ocean, the wind-driven upwelling and resultant hydrographic and biological patterns are also interlaced with large-scale non-local forcing in a complex and non-linear way (Strub et al., 1990; Hill et al., 1997). The anomalous Chl-*a* event in 1998 encouraged the investigation of a significant relationship with the most anomalous climatic event of the century; the 1997–1999 ENSO (McPhaden, 1999). Inverse relationships between the seasonally averaged Chl-*a* anomaly and wind-stress anomaly with MEI were mutually consistent (Fig. 6) and supported the existence of a link between ENSO and the strength of upwelling (and Chl-*a* blooms) through an atmospheric teleconnection. A significantly negative autumn–winter MEI value indicated an ongoing

mature phase of La Niña in the Pacific, resulting in a strengthening of the Atlantic trade winds in boreal winter–spring and vice-versa. A relaxed state of wind-forcing in the Mauritanian upwelling was found to intensify a few months later, following the summer–autumn El Niño–La Niña transition.

Although the Mauritanian upwelling is largely confined to the waters relatively close to the coast, its impact extends 300–600 km offshore, through Ekman flow, eddies and filaments (Mittelstaedt, 1991; Hill et al., 1998). A prominent cold filament permanently located at 21°N, which contributes to the entrainment of cold, nutrient-rich water from the coast up to 450 km offshore (Van Camp et al., 1991) is accompanied by another cold-core eddy between 10°N and 15°N (Fig. 7). The SLA and geostrophic current anomalies overlaid on Chl-*a* maps showed the extension of such persistent filaments in this region during the 1998–1999 anomalous months (Fig. 7). The transport of Chl-*a* offshore, possibly with nutrient-rich water,

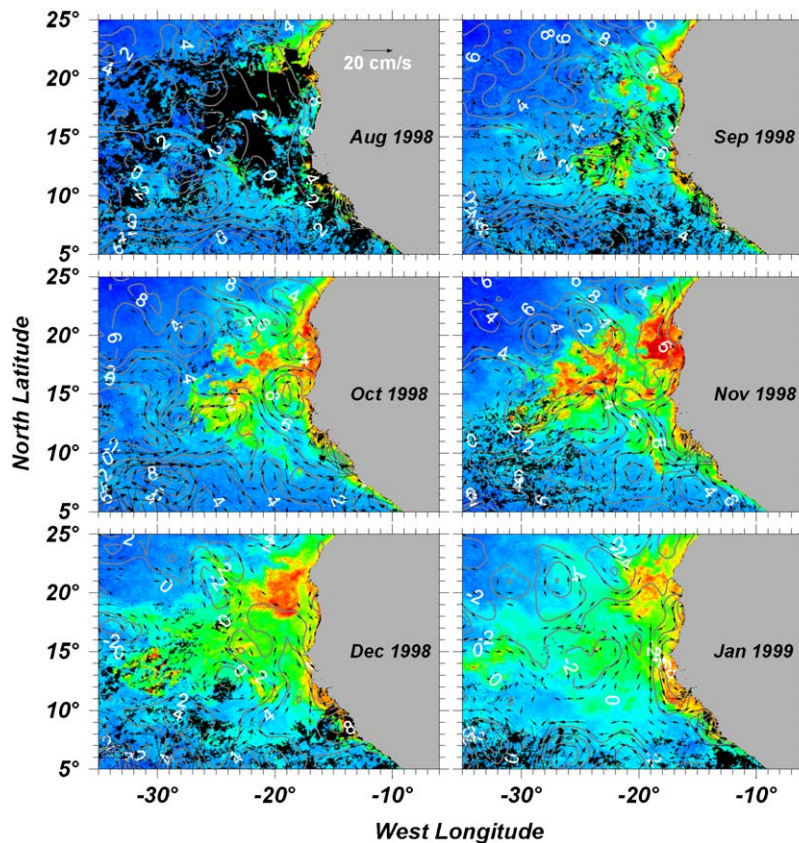


Fig. 7. Topex/Poseidon mean SLA (contours in cm; CI = 2 cm) and associated geostrophic current fields (vectors in cm s^{-1} ; vectors with magnitudes greater than 3 cm s^{-1} are plotted) superimposed on mean SeaWiFS Chl-*a* (colour scale same as in Fig. 1).

suggests that these processes could contribute at a scale much larger than the continental shelf. However, there was no concurrent drop in SST from satellite observations, although a strong zonal SST gradient in 1998–1999 along the northwest African coast has been reported elsewhere (Santos et al., 2005); perhaps the ENSO-related warming in the tropical Atlantic was responsible for the weak anti-correlation between Chl-*a* anomaly and SST anomaly in 1998 (not shown).

The entire northwest African coast is also influenced by the African desert dust transport, which supplements the levels of micronutrients (such as iron) to the adjacent marine ecosystem. Chiapello et al (2005) showed that satellite-derived dust optical thickness in 1998 over the northern tropical Atlantic was one of the most intense events in the last two decades. Although the dust is transported at higher altitudes in summer, it is more likely that the winter transport corresponds to a settling in the Atlantic Ocean (I. Chiapello, pers. comm.). Whilst the contribution of wind-driven upwelling is significantly correlated to the Chl-*a* anomalies in the Mauritanian upwelling, an increased level of surface micronutrients (iron) arising from the winter Saharan dust deposition may also explain the anomalous bloom in 1998. Since the long-term variability of wintertime African dust transport is influenced by the North Atlantic Oscillation (Chiapello et al., 2005), it will be possible to investigate the decadal changes (regime shift) of Chl-*a* concentration in the Mauritanian upwelling when a longer consistent ocean-colour data record is available.

5. Conclusions

This study has verified that wind-driven upwelling is the principal mechanism that controls the seasonal cycle and inter-annual variability of surface Chl-*a* concentration in the Mauritanian upwelling. The biological response to the strength of the alongshore wind-stress anomaly is coherent; it explains more than 40% of the regression variance ($r = -0.65$, $p < 0.001$). A delayed response (1–2 months) of the Chl-*a* anomaly to the wind-stress curl anomaly was also found to be highly correlated ($r = 0.66$, $p < 0.001$). These two principal physical forcing functions (τ_y and $\nabla \times \tau$) jointly explained more than 50% of the Tchl-*a* variance. On a seasonal basis, coastal upwelling (Ekman suction) appeared to be significantly related ($|r| > 0.5$,

$p < 0.01$) to the Chl-*a* variability during spring–summer (autumn–winter).

A moderate correlation ($r = -0.52$, $p < 0.01$) between summer–autumn MEI and the Mauritanian Chl-*a* anomaly during autumn–winter supported the ENSO-related atmospheric modulation in the tropical Atlantic. This large-scale forcing by the atmosphere altered the local wind fields that accounted for the observed surface Chl-*a* variability in the Mauritanian upwelling during 1998. ENSO-related variability is thus a preferred explanation for the local changes in the biological fields in the vicinity of the northwest African upwelling system.

Acknowledgements

We thank all crew members and scientists of AMT who collected and analysed the in situ data and brought them into a ready-to-use form. SeaWiFS data are provided by the SeaWiFS Project, NASA/Goddard Space Flight Center and ORBIMAGE. We thank J. Gunson, D. Sengupta, R. Murtugudde, D. Raitos and R. Pérez-Portela for their help; special thanks to I. Chiapello for useful discussion on the African dust transport in the tropical Atlantic. Critical comments by two anonymous reviewers helped to improve an earlier version of the manuscript. This is contribution number 121 of the AMT programme and was funded through collaborative research within CASIX (publication number 41).

References

- Aiken, J., Bale, A.J., 2000. An introduction to the Atlantic meridional transect (AMT) programme. *Progress in Oceanography* 45 (3–4), 251–256.
- Aiken, J., Cummings, D.G., Gibb, S.W., Rees, N.W., Woodd-Walker, R., Woodward, E.M.S., Woolfenden, J., Hooker, S.B., Berthon, J.-F., Dempsey, C.D., Suggett, D.J., Wood, P., Donlon, C., Gonzalez-Benitez, N., Huskin, I., Quevedo, M., Barciela-Fernandez, R., Vargas, C.D., McKee, C., 1998. AMT5 cruise report. In: Firestone, E.R. (Ed.), NASA Tech. Memo. 1998-206892, vol.2. NASA Goddard Space Flight Center, Greenbelt, MD, p. 113p.
- Altman, D.G., 1991. *Practical Statistics for Medical Research*. Chapman & Hall, London, 611pp.
- Bakun, A., Nelson, C.S., 1991. The seasonal cycle of wind-stress curl in subtropical eastern boundary current regions. *Journal of Physical Oceanography* 21 (12), 1815–1834.
- Carr, M.-E., 2001. Estimation of potential productivity in eastern boundary currents using remote sensing. *Deep-Sea Research II* 49 (1–3), 59–80.
- Chavez, F.P., Strutton, P.G., Friederich, C.E., Feely, R.A., Feldman, G.C., Foley, D.C., McPhaden, M.J., 1999.

- Biological and chemical response of the equatorial Pacific Ocean to the 1997–1998 El Niño. *Science* 286 (5447), 2126–2131.
- Chiappello, I., Moulin, C., Prospero, J.M., 2005. Understanding the long-term variability of African dust transport across the Atlantic as recorded in both Barbados surface concentrations and large-scale total ozone mapping spectrometer (TOMS) optical thickness. *Journal of Geophysical Research* 110 (D18) (article no.-D18S10).
- Cipollini, P., Cromwell, D., Challenor, P.G., Raffaglio, S., 2001. Rossby waves detected in global ocean colour data. *Geophysical Research Letters* 28 (2), 323–326.
- Dandonneau, Y., Deschamps, P.-Y., Nicolas, J.-M., Loisel, H., Blanchot, J., Montel, Y., Thieuleux, F., Becu, G., 2004. Seasonal and inter-annual variability of ocean color and composition of phytoplankton communities in the north Atlantic, equatorial Pacific and south Pacific. *Deep Sea Research II* 51 (1–3), 303–318.
- Hill, A.E., Brown, J., Fernand, L., 1997. The summer gyre in the western Irish sea: shelf sea paradigms and management implications. *Estuarine Coastal and Shelf Sciences* 44 (Suppl. A), 83–95.
- Hill, A.E., Hickey, B.M., Shillington, F.A., Strub, P.T., Brink, K.H., Barton, E.D., Thomas, A.C., 1998. Eastern ocean boundaries. Coastal segment (E). In: Robinson, A.R., Brink, K.H. (Eds.), *The Sea, the Global Coastal Ocean: Regional Studies and Syntheses*, vol. 11. Wiley, New York, pp. 29–67.
- Huang, H.-P., Kushnir, Y., Robertson, A.W., 2005. Atlantic SST gradient and the influence of ENSO. *Geophysical Research Letters* 32 (20), 1–4.
- Huberty, C.J., 2003. Multiple correlation versus multiple regression. *Educational and Psychological Measurement* 63 (2), 271–278.
- Larkin, N.K., Harrison, D.E., 2005. Global seasonal temperature and precipitation anomalies during El Niño autumn and winter. *Geophysical Research Letters* 32 (16), 1–4.
- McClain, C.R., Firestone, J., 1993. An investigation of Ekman upwelling in the North-Atlantic. *Journal of Geophysical Research—Oceans* 98 (C7), 12327–12339.
- McPhaden, M.J., 1999. Genesis and evolution of the 1997–98 El Niño. *Science* 283, 950–954.
- Mittelstaedt, E., 1991. The ocean boundary along the northwest African coast—circulation and oceanographic properties at the sea-surface. *Progress in Oceanography* 26 (4), 307–355.
- Monterey, G.I., Levitus, S., 1997. *Climatological Cycle of Mixed Layer Depth in the World Ocean*. NOAA NESDIS, US Government Printing Office, 5pp.
- Mueller, J.L., Bidigare, R.R., Trees, C., Balch, W.M., Dore, J., Drapeau, D.T., Karl, D., VanHeukelem, L., Perl, J., 2003. Ocean optics protocols for satellite ocean color sensor validation. In: *Biogeochemical and Bio-optical Measurements and Data Analysis Protocols*. NASA Technical Memorandum 2003–211621, Rev. 5, vol. V. NASA Goddard Space Flight Center, Greenbelt.
- Murtugudde, R.G., Signorini, S.R., Christian, J.R., Busalacchi, A.J., McClain, C.R., Picaut, J., 1999. Ocean color variability of the tropical Indo-Pacific basin observed by SeaWiFS during 1997–1998. *Journal of Geophysical Research—Oceans* 104 (C8), 18351–18366.
- O'Reilly, J.E., Maritorena, S., O'Brien, M.C., Siegel, D.A., Toole, D., Menzies, D., Smith, R.C., Mueller, J.L., Mitchell, B.G., Kahru, M., Chavez, F.P., Strutton, P., Cota, G.F., Hooker, S.B., McClain, C.R., Carder, K.L., Muller-Karger, F., Harding, L., Magnuson, A., Phinney, D., Moore, G.F., Aiken, J., Arrigo, K.R., Letelier, R., Culver, M., 2000. SeaWiFS postlaunch calibration and validation analyses. Part 3. NASA Technical Memorandum—SeaWiFS Postlaunch Technical Report Series 11, 1–49.
- Reynolds, R.W., Smith, T.M., 1994. Improved global sea surface temperature analyses using optimum interpolation. *Journal of Climate* 7, 929–948.
- Roy, C., Reason, C., 2001. ENSO related modulation of coastal upwelling in the eastern Atlantic. *Progress in Oceanography* 49 (1–4), 245–255.
- Sætersdal, G., Bianchi, G., Strømme, T., Venema, S.C., 1999. The DR. FRIDTJOF NANSEN Programme 1975–1993. *Investigations of Fishery Resources in Developing Countries. History of the Programme and Review of Results*. FAO Fisheries Technical Paper 391. FAO, Rome.
- Santos, A.M.P., Kazmin, A.S., Peliz, A., 2005. Decadal changes in the Canary upwelling system as revealed by satellite observations: their impact on productivity. *Journal of Marine Research* 63 (2), 359–379.
- Siegel, D.A., 2001. Oceanography—the Rossby rototiller. *Nature* 409 (6820), 576–577.
- Signorini, S.R., Murtugudde, R.G., McClain, C.R., Christian, J.R., Picaut, J., Busalacchi, A.J., 1999. Biological and physical signatures in the tropical and subtropical Atlantic. *Journal of Geophysical Research* 104 (C8), 18367–18382.
- Stein, M.L., 1999. *Interpolation of Spatial Data: Some Theory for Kriging*. Springer Series in Statistics. Springer, Berlin, 275pp.
- Strub, P.T., James, C., Thomas, A.C., Abbott, M.R., 1990. Seasonal and nonseasonal variability of satellite-derived surface pigment concentration in the California current. *Journal of Geophysical Research* 95 (C7), 11501–11530.
- Thomas, A.C., Blanco, J.L., Carr, M.E., Strub, P.T., Osses, J., 2001a. Satellite-measured chlorophyll and temperature variability off northern Chile during the 1996–1998 La Niña and El Niño. *Journal of Geophysical Research* 106 (C1), 899–915.
- Thomas, A.C., Carr, M.-E., Strub, P.T., 2001b. Chlorophyll variability in eastern boundary currents. *Geophysical Research Letters* 28 (12), 3421–3424.
- Thomas, A.C., Strub, P.T., Carr, M.E., Weatherbee, R., 2004. Comparisons of chlorophyll variability between the four major global eastern boundary currents. *International Journal of Remote Sensing* 25 (7–8), 1443–1447.
- Tomczak, M., Godfrey, J.S., 1994. *Regional Oceanography: An Introduction*. Pergamon, Oxford, 442pp.
- Uz, B.M., Yoder, J.A., Osychny, V., 2001. Pumping of nutrients to ocean surface waters by the action of propagating planetary waves. *Nature* 409 (6820), 597–600.
- Van Camp, L., Nykjaer, L., Mittelstaedt, E., Schlittenhardt, P., 1991. Upwelling and boundary circulation off Northwest Africa as depicted by infrared and visible satellite observations. *Progress in Oceanography* 26 (4), 357–402.
- Wilson, C., Adamec, D., 2002. A global view of bio-physical coupling from SeaWiFS and TOPEX satellite data, 1997–2001. *Geophysical Research Letters* 29 (8) (article no.-1257).

- Wolter, K., 2006. Multivariate ENSO index (MEI). Climate Diagnostics Centre, NOAA Available from: <<http://www.cdc.noaa.gov/people/klaus.wolter/MEI/>>.
- Yamagata, T., Iizuka, S., 1995. Simulation of the tropical thermal domes in the Atlantic—a seasonal cycle. *Journal of Physical Oceanography* 25 (9), 2129–2140.
- Yelland, M., Taylor, P.K., 1996. Wind stress measurements from the open ocean. *Journal of Physical Oceanography* 26 (4), 541–558.
- Zhou, M., Paduan, J.D., Niiler, P.P., 2000. Surface currents in the Canary Basin from drifter observations. *Journal of Geophysical Research* 105 (C9), 21893–21911.